



# Unified Mathematic and Geometric Model of Cutting Edge Separation with Corner Radius in Turning

Storch Borys and Żurawski Łukasz<sup>(✉)</sup>

Faculty of Mechanical Engineering, Department of Engineering of Technical and Information Systems, Technical University of Koszalin, ul. Raclawicka 15-17, 75-620 Koszalin, Poland

lukasz.zurawski@tu.koszalin.pl

**Abstract.** In modern multiuse cutting tools with insert (e.g. with superfinishing edge or Wiper), such a cutting edge is made without documenting the basics for optimizing its dimensions. The article presents a generalized edge wear model in the surroundings of a rounded tip. In this sense the suggested solution is a novelty as it makes possible to specify the edge working conditions by modifying the edge corner and to adapt different tools for various cutting parameters established for creating a machined surface. The matter described in the article elaborates on patent number PL 173536 B1 where the usefulness of the solution for other tools (cutters, reamers, drills) was described. After the suggested works on the edge tip, due to the load along the cutting edge with the edge corner radius and along the cutting edge surface, always greater than zero and determining in both cases unit forces, it was possible to solve the mechanics of wear in the surroundings of the edge corner tip. The obtained model allows defining problems connected with the created unevenness on the machined surface. If plasticity phenomena in the cutting zone are taken into consideration, it can be proved that there is a group of wear marks after multiple passes of the edge tip in a disorganized random manner.

**Keywords:** Tool wear · Cutting edge · Corner radius · Turning

## 1 Introduction

The main objective of the article was to develop a new model of the course of wear of the clearance part located on corner top, which through its direct contact with the machined surface, exerts impact on creation of its surface.

As the cutting process progresses, marks of wear can be noticed on the tool's active surface [1, 2]. The marks image depends on how the tool angle is shaped geometrically. With a view on this, the most generic case of a tool with a circle-sector shaped edge was examined. The observed marks on a turning tool edge were depicted in Fig. 1. Three areas were marked on it, characterized by different mechanics and image of the marks. Differences between those images are seen between the areas I, II, III (Fig. 1). This depends on: cutting conditions, workpiece material of type, and strength of tool material. What needs to be mentioned here are the wear marks on the flank face or lack

of a grooved mark on the tool face. In the cut layer, under the curvature of the cutting edge, there is a layer of plastic deformed material and it is up to approximately 0,2 mm depth. The thickness of the layer is marked in Fig. 1 with a dotted line, while the area is spotted.

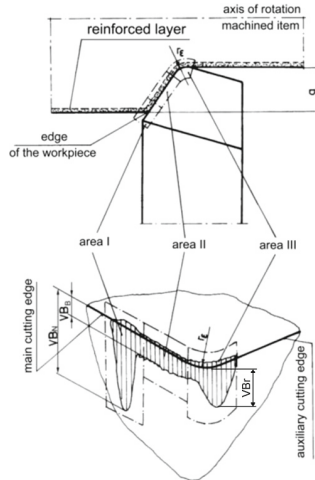


**Fig. 1.** Wear marks on the tool's working surfaces.

As the wear increases, a characteristic point where the cutting edge cuts the wrought layer appears in area I. The location of this point determines the cutting depth and a concentrated wear mark whose width is connected with the depth of the wrought layer appears around that point. The increased temperature in this area and the access of air from the edge open side intensify the wear growth, which manifests itself with a long local abrasion mark. In area II the abrasion adopts the shape of a rectangular strip that increases in width as the machining progresses. In area III the wear image is the result of highly complex mechanisms. In accordance with the previously discussed model, what is undergoing changes in the cutting zone is the layer thickness so that  $h < h_{\min}$ . This happens in particular when the feed ( $f$ ) is less than 0,2 mm per revolution, i.e.  $f < 0,2$  mm/rev). [5, 6]. The mechanics of changes in tool edge apex geometry were examined for such geometric conditions.

A few articles have attempted to explain the cutting edge operation. The findings in [3] regarding the solution of turning tool wear are limited to value  $VB$ . This review covers cutting operation on its main cutting surface and reports on  $VBA$ ,  $B$ ,  $C$ , and  $N$ . Whereas, the auxiliary cutting surface describes  $VB_r$ .

Value of  $VB$  wear does not influence the surface roughness parameters, while  $VB_r$  directly modifies the unevenness set. The  $h$  adopted by the Author [4] does not take into consideration cutting force components, yet it considers only the geometric modeling. It specifically refers to cylindrical face milling, and not to turning [4].

The articles [7–9, 13–16] on cutting edge work and mathematical modeling of cutting forces describes the conditions during process milling. In the case of turning, the cutting

edge has been described but without the wear tool being consumed and without affecting the rounding radius of the cutting edge  $r_n$  [10–12]. In the other publications [17–21] the values of tool wear are presented but without describing their actual impact on the mechanism of separation with the wear tool. The papers [22–26] presents the corners radius of the tool  $r_n$ , but without referring to the limited possibility of chip formation due to the minimum thickness of the cutting layer, as shown in the previously publications [5, 6] especially in the vicinity of the corner tip of the tool and its image.

## 2 Analytical Model of Tool Wear

The following initial conditions were adopted to create the analytical tool wear model:

1. The tool has an edge with radius  $r_e$ ,
2. Flank surface is circumscribed with angles  $\alpha_p$  and  $\alpha_f$ ,
3. Rake surface is circumscribed with angle  $\gamma_f$ .

Apart from the geometric conditions it was assumed that, as a result of the wear, the tool is shortened by value  $KE$ . Angle  $\lambda_s$  would not contribute in any significant way to the discussion, but a correction including dislocation of the point on the tool edge apex has been included.

## 3 Geometry of the Tool Workpiece System

Generally, it can be assumed that the tool edge is a sector of a cylindrical surface with radius  $r_e$ . This results from the fact that in the tool system, radius  $r_e$  is shaped on a plane parallel to the basic plane. By grinding the main and auxiliary flank surface, the cylinder circumscribed on this edge is rotated in plane  $P_f$  by angle  $\alpha_f$  and in plane  $P_p$  by angle  $\alpha_p$ .

When turning, the workpiece is the cylinder surface with radius  $R = D/2$ . In relation to the cylinder, in accordance with the previous assumptions in the XYZ coordinate system, the cylinder circumscribed on edge with radius  $r_e$  was spatially oriented. The coordinate system axes traverse in such a way so that they intersect the symmetry axes of the adopted cylinders (Fig. 2a).

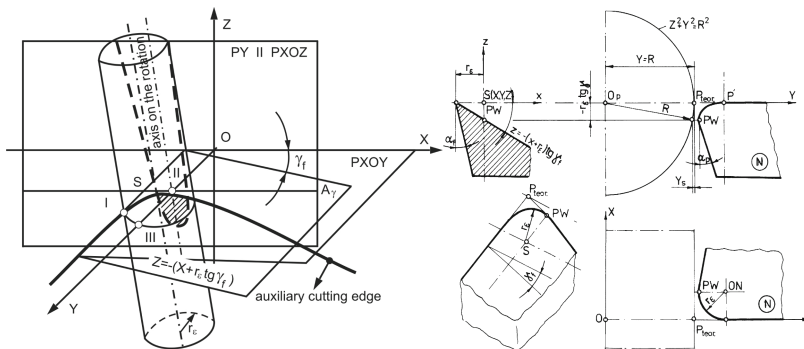


**Fig. 2.** a) simplified geometric model of cylinders intersecting, where one has radius  $R$ , b) location of the characteristic points on the tool edge in relation to the workpiece axis.

A circle, whose center lies in the place marked with  $S(S_x, S_y, S_z)$  point, was inscribed on the flank surface for  $\gamma_f > 0$  (Fig. 2b). Axis of the cylinder circumscribed on the tool apex also passes through this point. The distance between the cylinders' axes, considering the wear values and impact of the rake angle, will be:

$$S_y = R + r_\varepsilon - \Delta \quad (1)$$

In this Eq. (1), apart from the sum of cylinders' radiuses, there is a value marked with  $\Delta$  that is the sum of radial traverse, forced by the wear and  $Y_s$  adjustment caused by the rake angle  $\gamma_f$  (Fig. 2b). This results from the fact that when the rake angle is  $\gamma_f = 0$ , point  $P_{\max}$ , furthest on the edge tool apex, intersects with point  $P_{\text{teor}}$ , corresponding to the turning diameter. When rake angle  $\gamma_f \neq 0$  and tilt angle of the main cutting edge  $\lambda_s \neq 0$ , relevant tool traverse, which decreases the distance between cylinders' axes by value  $Y_s$ , needs to be taken into consideration. In the rear plane, in a section crossing through the apex point  $P_{\max}$ , when the value of abrasion  $VBr$  on flank surface is known, radial tool wear  $KE$  can be calculated on basis of the following relation (2):

$$KE = \frac{VB'r \operatorname{tg} \alpha_p}{1 - \operatorname{tg} \gamma_p \operatorname{tg} \alpha_p} \quad (2)$$

And the equations system (3) of solution is:

$$\left. \begin{aligned} Z^2 + Y^2 &= R^2 \\ Z &= -r_\varepsilon \operatorname{tg} \gamma_f \end{aligned} \right\} \quad (3)$$

We looked for point  $Y = Y_s$  (Fig. 2), by which an analytical axis distance must be shortened. During wear tool  $VBr$  (Fig. 1) on the corner radius  $r_\varepsilon$ , which is expected value  $Y_s$ , then shortened by on value  $KE$  (2).

Then we get the final Eq. (4) is therefore the sum of Eqs. (2) and (3).

From Eq. (4)  $Y_s$  allows to explain the distance between the axis of the rotation and the substitute plane  $PY$  II  $PXOZ$ .

Whereas  $Y = R$ , when  $R$  is half workpiece diameter  $D$  (Fig. 2).

$$Y_s = R - \sqrt{R^2 - r_\varepsilon^2 \operatorname{tg}^2 \gamma_f} \quad (4)$$

Equation of the circle in a plane parallel to the basic plane  $P_r$  with center coordinates  $S_x = 0, S_y = R + r_\varepsilon - \Delta, S_z = 0$  in accordance with the system in Fig. 2a, can be written down as follows:

$$X^2 + [Y - (R + r_\varepsilon - \Delta)]^2 = r_\varepsilon^2 \quad (5)$$

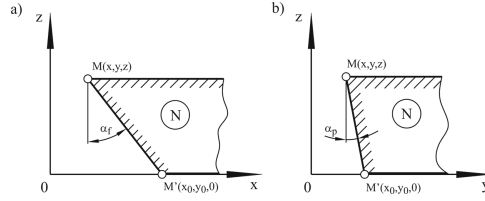


**Fig. 3.** Auxiliary diagrams for determining equations of the cylinder's generating lines: a) after rotating the line by angle  $\alpha_f$ , b) after rotating by angle  $\alpha_p$ .

On plane XOZ the cylinder is rotated by angle  $\alpha_f$ , therefore the generating line of the cylinder should cross axis Z at this angle, as demonstrated in Fig. 3a. Similarly, in plane YOZ, the cylinder's generating line is rotated by angle  $\alpha_p$ . Equation of the line passing through two points M and M', which is also the equation of the cylinder generating line, can be drawn from the following relation (6) and (7):

$$\frac{X_0 - X}{0 - Z} = \text{tg } \alpha_f \quad (6)$$

Where after conversion, expression for Z is determined

$$Z = \frac{X - X_0}{\text{tg } \alpha_f} \quad (7)$$

Relevant dependences, but in YOZ plane, give (8)

$$\frac{Y_0 - Y}{0 - Z} = \text{tg } \alpha_p \quad (8)$$

The final equation of line, crossing through points m and m' and rotated by angle  $\alpha_f$  and  $\alpha_p$  can be written down as (9):

$$Z = \frac{X - X_0}{\text{tg } \alpha_f} = \frac{Y_0 - Y}{\text{tg } \alpha_p} \quad (9)$$

After determining from the system of equations

$$\left. \begin{aligned} X &= X_0 + Z \text{tg } \alpha_f \\ Y &= Y_0 + Z \text{tg } \alpha_p \end{aligned} \right\} \quad (10)$$

And after replacing in the circle Eq. (3) the following is obtained Eq. (11)

$$(X_0 + Z \text{tg } \alpha_f)^2 + (Y_0 + Z \text{tg } \alpha_p - R - r_\varepsilon + KE + Y_s)^2 = r_\varepsilon^2 \quad (11)$$

When each point on the generating line also lies on the cylinder's surface in the adopted tool - workpiece system (Fig. 2a), and the equation of the cylinder circumscribing the workpiece machined surface has the following form:

$$\left. \begin{aligned} Z^2 + Y^2 &= R^2 \\ (X + Z \cdot \text{tg } \alpha_f)^2 + (Y + Z \cdot \text{tg } \alpha_p - R - r_\varepsilon + KE + Y_s) &= r_\varepsilon^2 \end{aligned} \right\} \quad (12)$$

Then the solution is a closed space curve which is the edge of intersection of intersecting cylinders. The equations obtained as a result of equation conversion (2) expression

$$Y = \sqrt{R^2 - Z^2} \quad (13)$$

replaced in Eq. (12) cannot be ousted and for this reason the system of Eqs. (12) is difficult to solve. The solution can be facilitated by adopting known values of variable  $Z$  from the range of  $-R < Z < +R$   $Z$  values, for which discrimination of quadratic equation is greater than zero, in the field of  $X, Y, Z$  data for the cylinders intersecting curve.

#### 4 Simplified Case of Tool - Workpiece System

Due to the complex form of general Eqs. (12), a different geometric model of the tool - workpiece system was adopted (Fig. 2a). When the ratio of radiuses  $r_\varepsilon$  to  $R$  is low, then it can be assumed that the cylinder circumscribed on the apex radius is cut with  $PY$  plane, parallel to  $PXOZ$  place. The  $PY$  plane was placed at a distance  $Y = R$  from the beginning of the coordinates system. Just like previously, a cylindrical surface rotated at angles  $\alpha_f$  and  $\alpha_p$  can be led through the edge tool, before the wear out of the object traversed by the distance  $Y = R$  to the workpiece (Fig. 2a). Therefore, the cylindrical surface equation will have the following form (14)

$$(X + Z \operatorname{tg} \alpha_f)^2 + (Y + Z \operatorname{tg} \alpha_p - R - r_\varepsilon + KE + Ys)^2 = r_\varepsilon^2 \quad (14)$$

where all variables are the same, just as in Eq. (12).

After replacement of value  $Y = R$ , i.e. after intersecting the cylindrical surface (14) with place  $PY$ , the following is obtained

$$(X + Z \operatorname{tg} \alpha_f)^2 + (Z \operatorname{tg} \alpha_p - r_\varepsilon + KE + Ys)^2 = r_\varepsilon^2 \quad (15)$$

After multiplying the components and comparing the general equation of a 2<sup>nd</sup> order curve

$$AX^2 + BXZ + CZ^2 + DX + EZ + F = 0 \quad (16)$$

With development of Eq. (14) the following was obtained:

$$A = 1 \quad (17)$$

$$B = 2 \operatorname{tg} \alpha_f \quad (18)$$

$$C = \operatorname{tg}^2 \alpha_p + \operatorname{tg}^2 \alpha_f \quad (19)$$

$$D = 0 \quad (20)$$

$$E = \operatorname{tg} \alpha_p (KE + Ys - r_\varepsilon) \quad (21)$$

$$F = (KE + Y_s - r_\varepsilon)^2 - r_\varepsilon^2 \tag{22}$$

then the examined equation invariants (16)

$$w = \begin{vmatrix} A & B \\ B & C \end{vmatrix} > 0 \tag{23}$$

$$W = \begin{vmatrix} A & B & D \\ B & C & E \\ D & E & F \end{vmatrix} < 0 \tag{24}$$

therefore, the value as well

$$AW < 0 \tag{25}$$

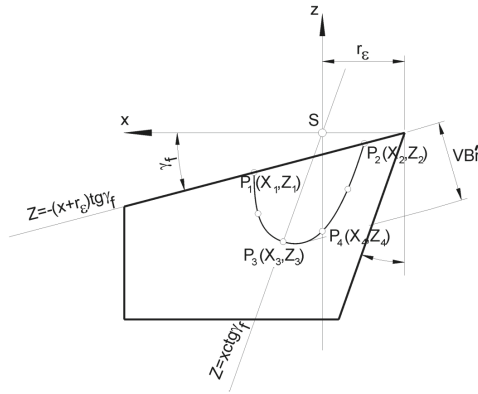


**Fig. 4.** Auxiliary diagram for calculating coordinates of the ellipse's characteristic points.

As a result, the obtained curve is the equation of the actual ellipse. After calculating the necessary auxiliary data and inserting them into the ellipse Eq. (15) characteristic points  $P_1, P_2, P_3$  and  $P_4$  can be established that describe the ellipse section, limited with rake surface, as illustrated in Fig. 4.

When the rake angle  $\gamma_f$  is greater than zero, equation of line which will be the edge of intersection of PY plane with the plane crossing through the rake surface needs to be inserted into (26), i.e.

$$Z = -(X + r_\varepsilon) \operatorname{tg} \gamma_f \tag{26}$$

Then the following equation is obtained

$$\begin{aligned} X^2 \left[ (1 - r_\varepsilon \operatorname{tg} \alpha_f \operatorname{tg} \gamma_f)^2 + \operatorname{tg}^2 \alpha_p \operatorname{tg}^2 \gamma_f \right] + X \left[ -(2r_\varepsilon (1 - \operatorname{tg} \alpha_f \operatorname{tg} \gamma_f) \operatorname{tg} \alpha_f \operatorname{tg} \gamma_f \right. \\ \left. + 2 \operatorname{tg} \alpha_p \operatorname{tg} \gamma_f (-r_\varepsilon \operatorname{tg} \alpha_f \operatorname{tg} \gamma_f - r_\varepsilon + KE + Y_s) + r_\varepsilon^2 \operatorname{tg}^2 \alpha_f \operatorname{tg}^2 \gamma_f \right. \\ \left. + (-r_\varepsilon \operatorname{tg} \alpha_f \operatorname{tg} \gamma_f - r_\varepsilon + KE + Y_s)^2 - r_\varepsilon^2 \right] = 0 \end{aligned} \tag{27}$$

After introducing auxiliary designations

$$A = [1 - r_\varepsilon \operatorname{tg} \alpha_f \operatorname{tg} \gamma_f]^2 + \operatorname{tg}^2 \alpha_p \operatorname{tg}^2 \gamma_f \quad (28)$$

$$B = [-2r_\varepsilon(1 - \operatorname{tg} \alpha_f \operatorname{tg} \gamma_f) \operatorname{tg} \alpha_f \operatorname{tg} \gamma_f + 2 \operatorname{tg} \alpha_p \operatorname{tg} \gamma_f (-r_\varepsilon \operatorname{tg} \alpha_f \operatorname{tg} \gamma_f - r_\varepsilon + KE + Y_s)] \quad (29)$$

$$C = r_\varepsilon^2 \operatorname{tg}^2 \alpha_f \operatorname{tg}^2 \gamma_f + (-r_\varepsilon \operatorname{tg} \alpha_f \operatorname{tg} \gamma_f - r_\varepsilon + KE + Y_s)^2 - r_\varepsilon^2 \quad (30)$$

Equation (27) is reduced to the form

$$A X^2 + BX + C = 0 \quad (31)$$

Task roots (31)

$$X_{1,2} = \frac{-B \mp \sqrt{B^2 - 4AC}}{2A} \quad (32)$$

introduced into expression (26), makes it possible to calculate coordinates  $Z_1$  and  $Z_2$  of points  $P_1$  and  $P_2$  from Fig. 4.  $P_4$  point coordinates are determined after introducing into Eq. (15) coordinate  $X_4 = 0$  for point  $P_4$  and a second order equation is obtained:

$$Z_4^2 (\operatorname{tg}^2 \alpha_f + \operatorname{tg}^2 \alpha_p) - 2 Z_4 \operatorname{tg} \alpha_p (r_\varepsilon - KE - Y_s) + (r_\varepsilon - KE - Y_s)^2 - r_\varepsilon^2 = 0 \quad (33)$$

For point  $P_3$ , corresponding to intersection of the ellipse with its longer axis, after substituting equation of the line in Eq. (15)

$$Z = -X \operatorname{ctg} \alpha_f \quad (34)$$

Overlapping the axis, the following equation is obtained

$$X^2 \operatorname{tg}^2 \alpha_p \operatorname{ctg}^2 \alpha_f + 2X \operatorname{tg} \alpha_p \operatorname{ctg} \alpha_f (r_\varepsilon - KE - Y_s) + (r_\varepsilon - KE - Y_s)^2 - r_\varepsilon^2 = 0 \quad (35)$$

Roots of Eqs. (33) and (35) are the sought coordinates of points  $P_3$  and  $P_4$  of the ellipse fragment (Fig. 4). When angle  $\alpha_f$  is low, then the difference between the coordinates of points  $P_3$  and  $P_4$  is negligible in the calculations.

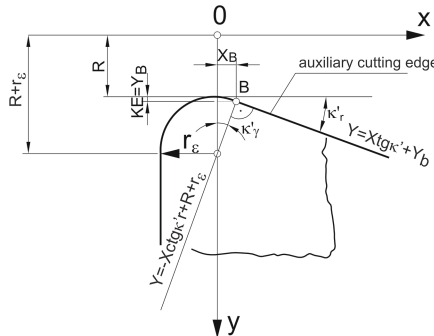


**Fig. 5.** Auxiliary diagram for calculating width of the abrasion mark on the transitory flank surface.



The auxiliary cutting edge is rectilinear and transforms into a curved edge in point B, as demonstrated in Fig. 5. When the axial tool wear KE obtains value higher than  $Y_B$ , it means that when

$$KE \geq Y_B \text{ dla } Y_B = r_\varepsilon(1 - \cos \kappa'_r) \tag{36}$$

then after substituting Eq. (2) in (36) the following is obtained

$$\frac{VBr \operatorname{tg} \alpha_p}{1 - \operatorname{tg} \gamma_p \operatorname{tg} \alpha_p} \geq r_\varepsilon(1 - \cos \kappa'_r) \tag{37}$$

In this expression VBr is the height of abrasion on the auxiliary flank surface. The obtained wear mark width  $X1 + X2$  (Fig. 4) will then be greater than results from solution (32), which is due to the fact that as the wear progresses, the point located on the circle moves onto the auxiliary edge.

### 5 Experimental Verification of Model Correctness

The interaction of friction surfaces, the cutting edge and machined material are accompanied by mutual wear. The abrasion on the corner radius is concentrated in a specific area. However, the phenomenon of friction in the area of common contact results in an unevenness image, as presented in Fig. 6. Growing abrasion marks are visible in a 50-times magnification.

This does not apply to the cracks depth, which are at least a grade smaller. This is irrelevant for our considerations as it would only hinder illustrating the issue with the descriptive method.

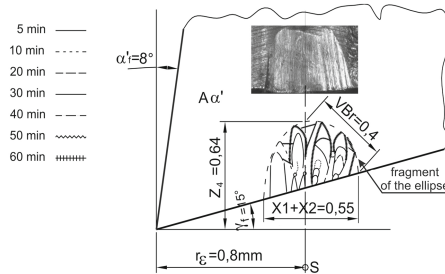


**Fig. 6.** Wear lands on transitional tool flank. Magnification 50×

In this work, the experimentally recorded curves of the abrasion ellipses corresponding to subsequent wear stages are plotted on the projection.

In Fig. 7 the corner wear image and machined surface fragment were put together. This figure shows the resemblance of the observed images that were collected while illuminating them with two light beams – blue and red.

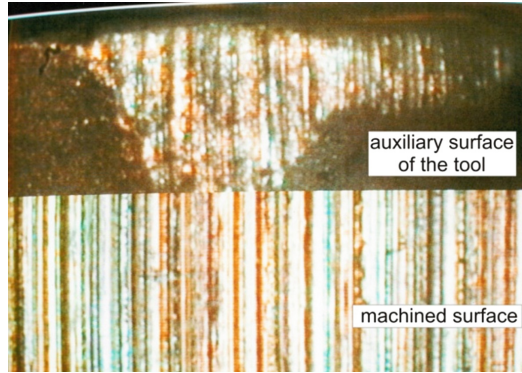


**Fig. 7.** Composition of two images: image of wear traces on the tip of cutting part and corresponding image of traces on the machined surface

It should be noted that many more details are made visible with the optic method, in contrast to 2D or 3D records on profilometers. The wear marks measured by increasing cutting time present a growth in the abrasion dimensions, which was presented in Fig. 8 as an example.

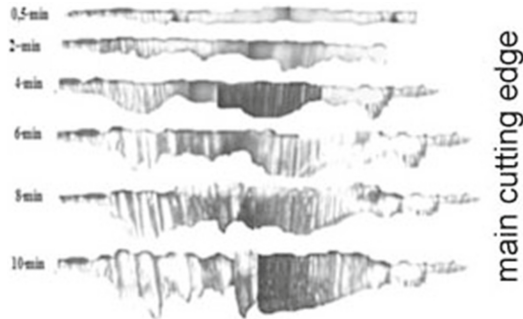


**Fig. 8.** Summary of wear marks, along the rounding of the corner radius for different cutting times

## 6 Conclusions

The vast amount of literature data concerning VBr changes that are dependent on time has encouraged the Authors to write down the following conclusions, focusing especially on some new aspects:

1. Solutions of the equations allow us to generalize the model of contact of two warped rollers and changes in the location of their axes towards one another due to the progressing tool wear.

2. The distance between the axes remains unchanged and wear of one of them changes the contact area.
3. As seen on the model, unevennesses in the diffusion area that make up the surface roughness have been modified.
4. This results from multiple passes of the machined surface across the abrasion width at the edge of top (Fig. 7 and 8).

## References

1. Brammertz, P.H.: Die Entstehung der Oberflächenerauheit beim Feindreihen, *Industrie Anzeiger*, 2 (1961)
2. Gieszen, C.A.: Bas seitliche Verguetschen des Werkstoffes auf den Oberflächen feingedrehter Werkstücke, *Fertigung*, 5 (1971)
3. Mikołajczyk, T., Nowicki, K., Kłodowski, A., Pimenov, D.Y.: Neural network approach for automatic image analysis of cutting edge wear. *Mech. Syst. Signal Process.* **88**, 100–110 (2017)
4. Pimenov, D.Y.: Geometric model of height of microroughness on machined surface taking into account wear of face mill teeth. *J. Frict. Wear* **34**(4), 290–293 (2013)
5. Storch, B., Zawada-Tomkiewicz, A.: Distribution of unit forces on the tool edge rounding in the case of finishing turning. *Int. J. Adv. Manuf. Technol.* **60**(5–8), 453–461 (2012)
6. Storch, B., Zawada-Tomkiewicz, A.: Distribution of unit forces on the tool nose rounding in the case of constrained turning. *Int. J. Mach. Tools Manuf.* **57**, 1–9 (2012)
7. Altintas, Y., Lee, P.: A general mechanics and dynamics model for helical end mills. *CIRP Ann.* **45**(1), 59–64 (1996)
8. Altintas, Y., Stepan, G., Merdol, D., Dombovari, Z.: Chatter stability of milling in frequency and discrete time domain. *CIRP J. Manuf. Sci. Technol.* **1**, 35–44 (2008)
9. Altintas, Y., Engin, S.: Generalized modeling of mechanics and dynamics of milling cutters. *CIRP Ann.* **50**(1), 25–30 (2001)
10. Altintas, Y., Kilic, Z.M.: Generalized dynamic model of metal cutting operations. *CIRP Ann. – Manuf. Technol.* **62**, 47–50 (2013)
11. Kilic, Z.M., Altintas, Y.: Generalized mechanics and dynamics of metal cutting operations for unified simulations. *Int. J. Mach. Tools Manuf.* **104**, 1–13 (2016)
12. Kilic, Z.M., Altintas, Y.: Generalized modeling of cutting tool geometries for unified process simulation. *Int. J. Mach. Tools Manuf.* **104**, 14–25 (2016)
13. Lee, P., Altintas, Y.: Prediction of ball-end milling forces from orthogonal cutting data. *Int. J. Mach. Tools Manuf.* **36**(9), 1059–1072 (1996)
14. Larue, A., Altintas, Y.: Simulation of flank milling processes. *Int. J. Mach. Tools Manuf.* **45**, 549–559 (2005)
15. Kaymakci, M., Kilic, Z.M., Altintas, Y.: Unified cutting force model for turning, boring, drilling and milling operations. *Int. J. Mach. Tools Manuf.* **54–55**, 34–45 (2012)
16. Budak, E., Ozlu, E.: Development of a thermomechanical cutting process model for machining process simulations. *CIRP Ann. – Manuf. Technol.* **57**, 97–100 (2008)
17. Altintas, Y., Jin, X.: Mechanics of micro-milling with round edge tools. *CIRP Ann. – Manuf. Technol.* **60**, 77–80 (2011)
18. Liu, Q., Altintas, Y.: On-line monitoring of flank wear in turning with multilayered feed-forward neural network. *Int. J. Mach. Tools Manuf.* **39**, 1945–1959 (1999)
19. Berenja, K.R., Karaa, M.E., Budak, E.: Investigating high productivity conditions for turn-milling in comparison to conventional turning. *Procedia CIRP* **77**, 259–262 (2018)

20. Bagherzadeh, A., Budak, E.: Investigation of machinability in turning of difficult-to-cut materials using a new cryogenic cooling approach. *Tribol. Int.* **119**, 510–520 (2018)
21. Olgun, U., Budak, E.: Machining of difficult-to-cut-alloys using rotary turning tools. *Procedia CIRP* **8**, 81–87 (2013)
22. Jin, X., Altintas, Y.: Prediction of micro-milling forces with finite element method. *J. Mater. Process. Technol.* **212**, 542–552 (2012)
23. Jin, X., Altintas, Y.: Slip-line field model of micro-cutting process with round tool edge effect. *J. Mater. Process. Technol.* **211**, 339–355 (2011)
24. Karaguzela, U., Uysalb, E., Budak, E., Bakkal, M.: Effects of tool axis offset in turn-milling process. *J. Mater. Process. Technol.* **231**, 239–247 (2016)
25. Celebia, C., Özlüb, E., Budak, E.: Modeling and experimental investigation of edge hone and flank contact effects in metal cutting. *Procedia CIRP* **8**, 194–199 (2013)
26. Budak, E., Ozlu, E., Bakioglu, H., Barzegar, Z.: Thermo-mechanical modeling of the third deformation zone in machining for prediction of cutting forces. *CIRP Ann. – Manuf. Technol.* **65**, 121–124 (2016)